Manganese induces oligomerization to promote down-regulation of the intracellular trafficking receptor used by Shiga toxin

Ritika Tewari, Timothy Jarvela, and Adam D. Linstedt
Department of Biological Sciences, Carnegie Mellon University, Pittsburgh, PA 15213

ABSTRACT **Manganese (Mn) protects cells against lethal doses of purified Shiga toxin by causing the degradation of the cycling transmembrane protein GPP130, which the toxin uses as a trafficking receptor. Mn-induced GPP130 down-regulation, in addition to being a potential therapeutic approach against Shiga toxicosis, is a model for the study of metal-regulated protein sorting. Significantly, however, the mechanism by which Mn regulates GPP130 trafficking is unknown. Here we show that a transferable trafficking determinant within GPP130 bound Mn and that Mn binding induced GPP130 oligomerization in the Golgi. Alanine substitutions blocking Mn binding abrogated both oligomerization of GPP130 and GPP130 sorting from the Golgi to lysosomes. Further, oligomerization was sufficient because forced aggregation, using a drug-controlled polymerization domain, redirected GPP130 to lysosomes in the absence of Mn. These experiments reveal metal-induced oligomerization as a Golgi sorting mechanism for a medically relevant receptor for Shiga toxin.**

Monitoring Editor
Keith E. Mostov
University of California, San Francisco

Received: May 22, 2014
Revised: Jul 16, 2014
Accepted: Jul 18, 2014

INTRODUCTION

Shiga infections involve life-threatening diarrhea, dysentery, and hemorrhagic colitis, all of which can lead to fatal hemorrhagic uremic syndrome (Beddoe *et al.*, 2010). There are few treatment options, and they are indirect, mostly involving hydration. Shiga belongs to the AB_5 class of bacterial toxins comprised of catalytic A subunits carried into cells by their associated homopentameric B subunits (Sandvig *et al.*, 2010). These toxins invade host cells by a retrograde route involving endocytosis, transport via the Golgi to the endoplasmic reticulum (ER), and translocation of the A subunit out of the ER to the cytoplasm (Mallard and Johannes, 2003). In the case of Shiga toxin, the A subunit causes cytotoxicity by inactivating ribosomes to shut down host cell protein synthesis (Endo *et al.*, 1988; Fraser *et al.*, 1994).

As it invades host cells, Shiga toxin avoids degradation in lysosomes by sorting into endosomal membrane tubules that move directly to the Golgi (Johannes and Wunder, 2011). For two major isoforms of Shiga toxin, STx (present in *Shigella*) and STx1 (present in strains of *Escherichia coli*), sorting into endosomal tubules is mediated by their binding to GPP130, a host cell transmembrane protein that constitutively cycles between endosomes and the Golgi (Mukhopadhyay and Linstedt, 2012). A binding site on the outer sidewall of the doughnut-shaped toxin B subunit engages a site near the membrane of the lumenal stem domain of GPP130, which is predicted to form a homodimeric coiled-coil (Mukhopadhyay *et al.*, 2013). In this way it is believed that STx/STx1 piggybacks a ride to the Golgi.

Therapeutic approaches that block toxin sorting in endosomes serve the dual purposes of blocking toxin movement to the Golgi and diverting it to lysosomes, where it is degraded and cleared from infected cells (Mukhopadhyay and Linstedt, 2013). Thus it is serendipitous that a relatively moderate increase in extracellular manganese (Mn) down-regulates GPP130 levels (Mukhopadhyay *et al.*, 2010). Indeed, nontoxic doses of Mn block STx/STx1 trafficking to the Golgi, cause toxin degradation in lysosomes, and prevent fatal toxicosis in both cultured-cell and mouse models (Mukhopadhyay and Linstedt, 2012).

GPP130 down-regulation by elevated extracellular Mn involves rab7-dependent movement of GPP130 from the Golgi to multivesicular bodies (MVBs) and lysosomes (Mukhopadhyay *et al.*, 2010). This response requires the Golgi-localized Ca^{2+}/Mn^{2+} pump SPCA1, indicating that it is increased Mn in the Golgi, which alters GPP130

This article was published online ahead of print in MBoC in Press (http://www.molbiolcell.org/cgi/doi/10.1091/mbc.E14-05-1003) on July 30, 2014.

Address correspondence to: Adam D. Linstedt (linstedt@andrew.cmu.edu).

Abbreviations used: AP, rapamycin analogue AP21998; DSP, dithiobis[succinimidyl propionate]; FM, $F_{36}M$ substitution of FKBP12; MVB, multivesicular body; NTA, nitrilotriacetic acid; TGN, *trans*-Golgi network.

sorting out of the *trans*-Golgi network (TGN). Although GPP130 is a unique example of Mn-sensitive trafficking in mammalian cells, there are important examples of altered membrane protein sorting by metal ions, particularly in relation to regulating ion homeostasis. Elevated copper causes the reversible redistribution of two copper transporters, ATP7A and ATP7B, from the TGN to the plasma membrane to expel copper and protect against its toxicity (La Fontaine and Mercer, 2007). Mutations of the transporters that block their altered trafficking have been identified, but the relevant target of copper and how it alters transporter TGN export remain unknown (Polishchuk and Lutsenko, 2013). Similarly, Mn homeostasis in *Saccharomyces cerevisiae* is controlled, in part, by trafficking of the Smf1p and Smf2p transporters (Reddi *et al.*, 2009). In the absence of Mn, the transporters traffic through the secretory pathway to the cell surface to scavenge any available ion. As Mn levels rise, the proteins are instead diverted to vacuoles, where they are degraded. Significant progress has been made on the mechanism of Smf1p/2p targeting to intraluminal vesicles of the MVB by ubiquitination (Sullivan *et al.*, 2007; Jensen *et al.*, 2009), but, again, the relevant target of the metal and how it alters TGN sorting are unknown.

Thus, although metal-induced changes in membrane trafficking are an important theme in ion homeostasis, there is a strong need for understanding the key step in which the metal is sensed and the signal is propagated to change sorting. To bind at low metal concentrations, constitutively occupied metalloproteins use high-affinity sites involving an array of coordinating charged side chains (Borgstahl *et al.*, 1992). In contrast, a protein that binds and responds to elevated metal concentrations might exhibit weaker affinity, perhaps by only partially coordinating the ion. Given the importance of identifying a metalloprotein undergoing metal-regulated sorting, we sought to determine whether Mn binds GPP130 and, if so, how it might alter GPP130 sorting. Our results indicate that GPP130 does interact directly with Mn, and this interaction causes a dramatic change in its assembly state both in vitro and in living cells. Further, this is required and sufficient to down-regulate the protein.

RESULTS

Mn-sensitive determinant

Our previous work showed that the GPP130 lumenal stem domain conferred Mn-sensitive targeting when appended to GP73, a structurally similar *cis*-Golgi protein whose trafficking is otherwise not altered by Mn (Mukhopadhyay *et al.*, 2010). Within the lumenal stem domain the juxtamembrane residues 36–175 were identified as important and became our focus in the present study. To further map residues conferring Mn sensitivity, we positioned a series of GPP130 sequence segments from this region between the GP73 N-terminus (containing its cytoplasmic, transmembrane, and stem domain) and green fluorescent protein (GFP). These chimeric proteins were expressed in HeLa cells. Mn sensitivity was measured by the ability of the transfected constructs to begin redistributing to endosomal structures in response to a 2-h exposure to a nontoxic dose of 500 μM $MnCl_2$. This time point is before substantial GPP130 degradation occurs and leaves a large amount of GPP130 in the Golgi, aiding the identification and quantification of the transfected cells. Thresholded images are presented to more readily visualize peripheral GPP130 punctae, which is necessary because GPP130 redistributes to MVB/lysosomes, where it is degraded relatively rapidly (Mukhopadhyay *et al.*, 2010). Images were also quantified to determine the number of non-Golgi puncta in the presence or absence of Mn. A pretreatment of cycloheximide for 2 h was used to prevent overexpression and deplete any ER pool of protein. Endogenous GPP130, detected with a non–cross-reacting antibody, was used to confirm an intact Mn response in the same cells.

Figure 1 shows the localization of a few key constructs before and after Mn (Figure 1A), as well as schematic depictions of the tested GPP130 segments together with their quantified presence in peripheral punctae (Figure 1B). Consistent with our previous work (Mukhopadhyay *et al.*, 2010), residues 36–175 produced a strong response, shifting from fewer than 5 non-Golgi puncta/cell in the absence of Mn to >30 puncta/cell in the presence of Mn. As noted before (Mukhopadhyay *et al.*, 2010), most of the puncta contained redistributed endogenous GPP130, whereas not all endogenous GPP130 puncta were positive for the transfected construct. C-terminal deletion generated constructs 36–107, 36–100, 36–95, and 36–87. All of these except 36–87 retained activity, indicating that residues 88–95 were critical. A similar set of N-terminal truncations indicated that the first 14 residues (36–49) were dispensable, with larger deletions causing loss of Mn-response activity. This left 50–95 as the minimal mapped region and the sequence stretch 88–95 as a tractable segment for point mutation. Several individual and combined alanine substitutions within 88–95 were without effect, but alanine substitution of the sequence $_{88}$DFLV$_{91}$ to generate 36-95-$_{88}$AAAA$_{91}$ potently blocked activity. This nonresponsive construct was stable and well localized and did not prevent the endogenous GPP130 response in the same cells. Insertion of the quadruple alanine substitution into the original construct to generate 36-175-$_{88}$AAAA$_{91}$ also strongly blocked its response (Figure 1). In summary, our mapping studies narrowed a transferable Mn responsive sequence to ~50 residues and identified a required sequence stretch that, when mutated, could be used as a critical negative control in subsequent experiments.

Mn binding and oligomerization

Based on the transferability of the Mn response, it seemed possible that the GPP130 stem domain might bind Mn. As a test, uncoated or Mn-coated nitrilotriacetic acid (NTA)-agarose beads were incubated with the purified glutathione *S*-transferase (GST)–tagged GPP130 residues 36–247, and recovery after washing was determined by SDS–PAGE and Coomassie staining. As control proteins we used GST itself and GST fused to the stem domain of GP73. The control proteins showed low recovery on the beads, whereas the GST-tagged GPP130 stem domain (36–175) appeared to interact strongly and specifically with the Mn-coated beads (Figure 2A). To estimate the Mn concentration required for half-maximal binding, we repeated the experiment by adding the GPP130 protein (36–247) to increasing concentrations of Mn and then recovering any formed complexes using uncoated NTA-agarose beads. Under these conditions, 0.4 mM Mn yielded half-maximal binding (Figure 2B). The concentration of Golgi Mn in Mn-treated cells is unknown. Because Mn is actively pumped into the Golgi, it seems reasonable that Mn exposure results in Golgi levels of Mn sufficient to bind the GPP130 stem domain. On the basis of these results, we next investigated Mn binding of the GPP130 stem domain using mutations based on two nonresponsive GPP130 constructs found in the trafficking assay. Therefore we purified GST-tagged 36-87 and 36-175-$_{88}$AAAA$_{91}$ and compared the binding of these proteins to uncoated and Mn-coated beads with that of the wild-type 36–175 construct. Each construct showed some recovery on Mn-coated beads, but the binding was >4.5-fold higher for the wild-type construct (Figure 2C). Thus maximal Mn binding in the assay required the same residues that are required for Mn responsiveness.

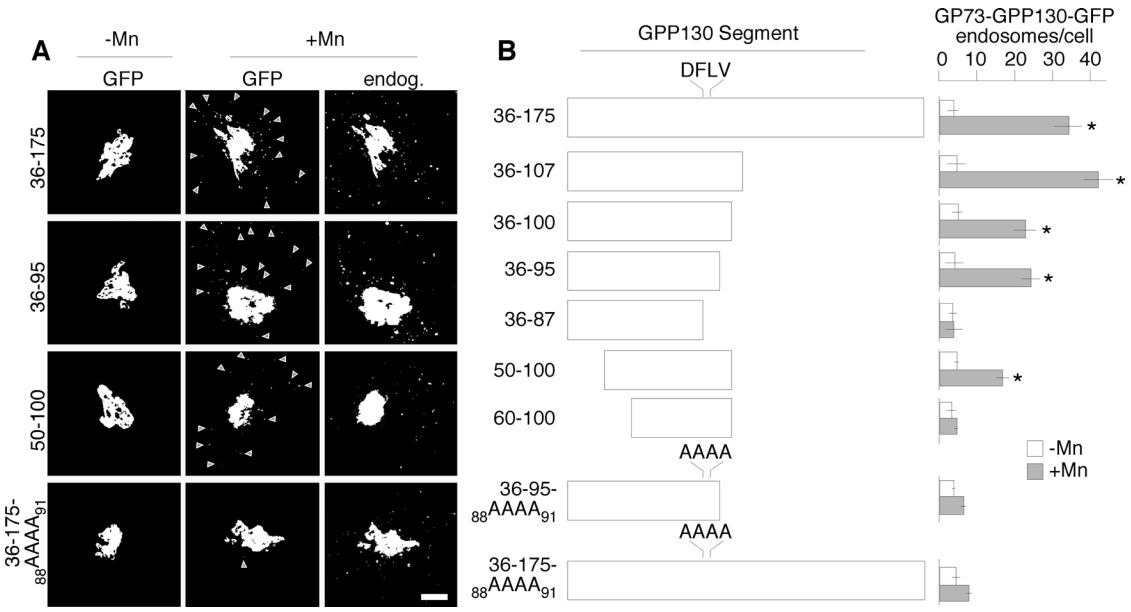

FIGURE 1: GPP130 lumenal sequence element confers Mn sensitivity. (A) Localization is shown for GFP-tagged GP73 constructs containing the indicated GPP130 residues in the absence or presence of 0.5 mM $MnCl_2$ for 2 h. The images are cropped and identically thresholded to accentuate presence in peripheral punctae. Arrowheads indicate the position of example punctae. The localization of endogenous GPP130 in the same Mn-treated cells serves as an internal control for the Mn response. The chimeric constructs contain the cytoplasmic, transmembrane, and stem domain of GP73, followed by a GPP130 segment, followed by GFP. Before analysis the cells were treated with 0.1 mg/ml cycloheximide for 2 h to prevent new synthesis. Scale bar, 5 μm. (B) Schematic diagram of the GPP130 segments present in the GFP-tagged GP73 chimeric constructs and the quantified determination of their presence in peripheral endosomal structures in the absence or presence of Mn. Object analysis is described in *Materials and Methods*. Values are averages ($n > 25$ cells, ±SEM). *$p < 0.05$ for comparison to untreated.

Of interest, the purified GPP130 stem domain constructs 36–247 and 36–175 appeared to oligomerize in response to Mn addition. In the absence of added Mn, GST-$GPP130_{36\text{-}247}$ was recovered roughly in the middle of velocity gradients, whereas addition of 1 mM $MnCl_2$ shifted ~60% of the protein toward the bottom of the gradients (Figure 3A). Mn-induced aggregation of the protein was also apparent simply by measuring absorbance at 350 nm, indicating light scattering (Cromwell *et al.*, 2006). Whereas the two purified control proteins, GST and GST-tagged GP73 stem, failed to show an increase, the GST-$GPP130_{36\text{-}247}$ protein yielded a robust increased absorbance clearly evident at 1 mM $MnCl_2$ (Figure 3B). This effect was reversible because it was abrogated by a subsequent incubation with equimolar EDTA to chelate the Mn (Figure 3C). Of importance, the alanine substitutions that blocked GPP130 responsiveness in cells and reduced binding of Mn in the GST-GPP130 stem construct (36-$175_{88}AAAA_{91}$) also reduced the Mn-induced light scattering activity of this construct (Figure 3D). These results suggest that Mn binding might promote altered GPP130 trafficking by binding and inducing GPP130 oligomerization.

Mn-induced oligomerization and trafficking

To test the hypothesis that Mn-induced oligomerization alters GPP130 trafficking, we first carried out cross-linking of untreated and Mn-treated cells using the membrane-permeant cross-linker dithiobis[succinimidyl propionate] (DSP). The Mn treatment was used to initiate GPP130 redistribution while leaving a substantial Golgi-localized pool. After cell lysis, the sedimentation behavior of endogenous GPP130 was determined on velocity gradients. In the absence of Mn, GPP130 was recovered near the top of the gradients, whereas Mn treatment resulted in recovery of almost 20% of the GPP130 in a much larger species near the bottom of the gradients (Figure 4A). Note that Mn was removed at the time of cross-linking and was absent for the remainder of the experiment, so the change in GPP130 behavior occurred in the intact cells. In addition, even in the absence of cross-linking, there was a reproducible, albeit small (5%), fraction of GPP130 in the bottom fractions of lysates from Mn-treated cells but not control cells (unpublished data). As a negative control, we also examined the behavior of endogenous GP73, which was recovered at the top of the gradients for both untreated and Mn-treated cells (Figure 4B). One concern was that the Mn-induced oligomerization of GPP130 might not be restricted to the Golgi. As a test, we carried out the cross-linking experiment on cells treated with Mn at 20°C to prevent GPP130 exit from the TGN. Immunofluorescence was used to confirm that 20°C incubation blocked redistribution of GPP130 into endosomes (unpublished data). Under these conditions, GPP130 was still recovered in the size-shifted fractions, indicating that oligomerization occurred in the Golgi (Figure 4C). Finally, we compared the oligomerization activity of the Mn-responsive wild-type GPP130 stem domain construct described earlier (Figure 1, residues 36–175 of GPP130 appended to the GP73 N-terminus) to the identically constructed protein containing the alanine substitutions that prevent Mn-induced trafficking to lysosomes (36-$175_{88}AAAA_{91}$). Whereas 20% of the 36–175 construct was recovered as a much larger species, the alanine-substituted construct was recovered exclusively in the top fractions of the gradients (Figure 4D).

Next we used fluorescence recovery after photobleaching (FRAP) to assess whether we could visualize an Mn-induced change in GPP130 diffusion in the Golgi. Cells were first transfected with a GFP-tagged GPP130 construct comprising the cytoplasmic,

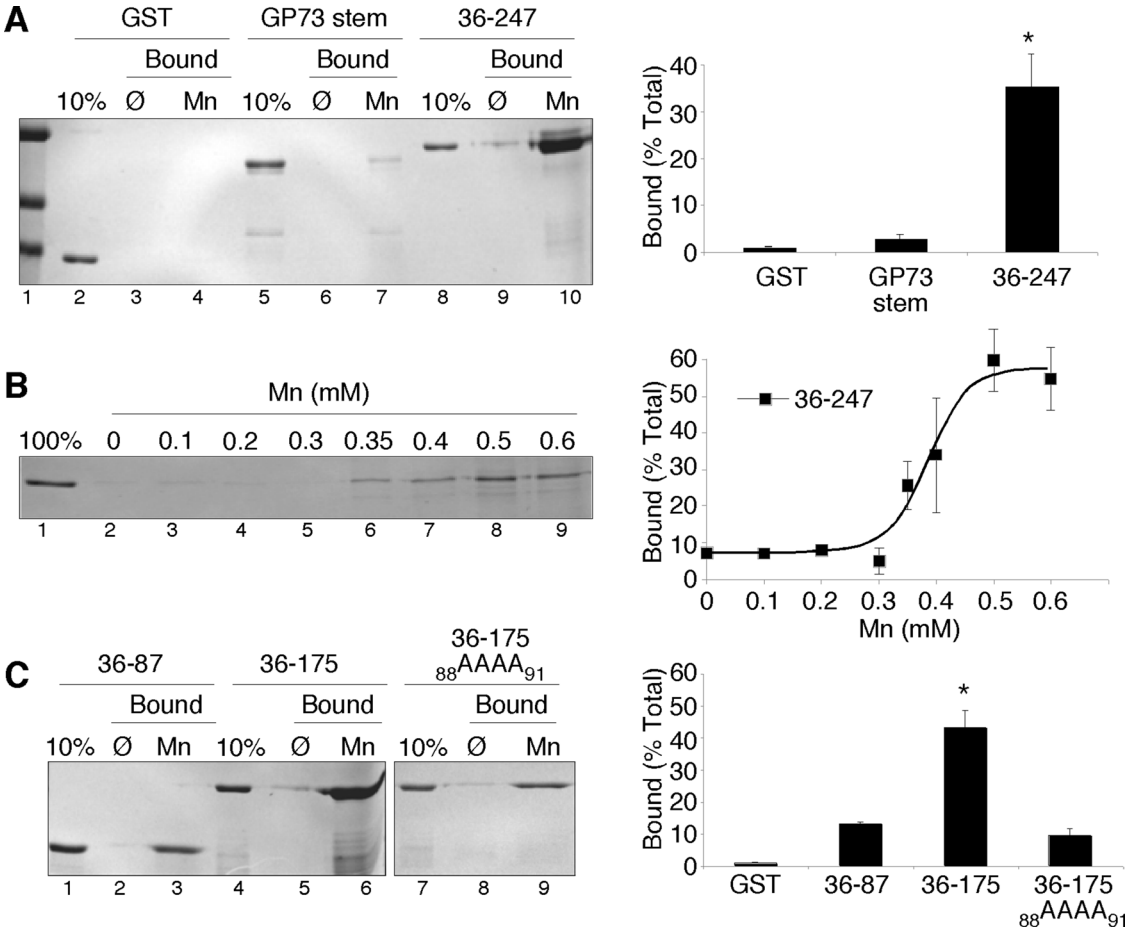

FIGURE 2: Mn binding by the GPP130 stem domain. (A) Recovery of purified GST, GST-tagged stem domain of GP73, or GST-tagged residues 36–247 of GPP130 on either uncoated or Mn-coated agarose beads. The Coomassie-stained gel also shows 10% of the total of each protein used in the binding assay. Quantification indicates the percentage bound to Mn-coated beads for each protein ($n = 3$, ±SEM). *$p < 0.05$ for comparison to other trials. (B) Coomassie-stained gel and quantification, indicating recovery of GST-tagged residues 36–247 of GPP130 after incubation with beads at the indicated concentrations of $MnCl_2$ ($n = 3$, ±SEM). (C) Recovery on uncoated or Mn-coated beads of purified GST-tagged GPP130 residues 36–87, 36–175, or 36–175 with the $_{88}AAAA_{91}$ substitution. Quantification of the Coomassie-stained gels is also shown for Mn-coated beads ($n = 3$, ±SEM). *$p < 0.05$ for comparison to other trials.

transmembrane, and stem domains and then were either untreated or treated with Mn. Again, a short-duration Mn exposure was used to initiate GPP130 redistribution but leave a substantial Golgi pool for analysis. A small region of this Golgi fluorescence was bleached, and recovery was determined over the next 10 min. Remarkably, the rapid recovery of GPP130 fluorescence in the Golgi of untreated control cells was significantly delayed in Mn-treated cells (Figure 5A). Quantification of fluorescence recovery in multiple independent trials confirmed that Mn induced a significant delay in GPP130 diffusion (Figure 5B). Note that in all other aspects, the Golgi fluorescence patterns of treated and untreated cells appeared indistinguishable. To test whether the blocking alanine substitutions would also prevent this Mn-induced delay in recovery, we repeated the experiments with the wild-type and alanine-substituted GP73-GPP130 chimeric constructs containing the GPP130 segment 36–175 followed by GFP. As expected, the wild-type construct rapidly recovered from photobleaching in the absence of Mn and showed a strong delay in recovery in Mn-treated cells (Figure 5C). In striking contrast to wild type, the $_{88}AAAA_{91}$ substitution completely abrogated the Mn-induced delay in diffusion, such that both untreated and treated cells exhibited identical recoveries (Figure 5D). The final extent of recovery for the alanine substitution also matched that of the wild-type construct in untreated cells. For an unknown reason, the extent of recovery of these chimeric constructs was lower than that observed for the GPP130 construct. Thus, in living cells, Mn induces a change in GPP130 diffusion in the Golgi that depends on the same residues implicated in Mn binding and Mn-induced oligomerization.

Oligomerization induces sorting to lysosomes

Because Mn alters GPP130 oligomerization status in the Golgi contemporaneous with Mn-induced movement of GPP130 to lysosomes, we next tested whether oligomerization is sufficient to cause sorting of GPP130 to lysosomes. Versions of GPP130 were constructed harboring an array of three copies of a modified version of a FKBP12 domain termed FM (after its $F_{36}M$ substitution) as previously described for the Golgi enzyme mannosidase 1 (Rizzo *et al.*, 2013). The FM domain self-interacts in a manner that is inhibited by the drug AP21998 (AP), an analogue of rapamycin. In the absence of AP, self-interactions are expected to form large complexes due to multiplexing of the three FM domains. In the previous work only 15 min of AP washout was needed to shift the FM-tagged mannosidase 1 from recovery in supernatant to pellet fractions (indicating polymerization), and this correlated with the construct's movement from *cis*- to *trans*-Golgi (Rizzo *et al.*, 2013). In the case of GPP130-$_{1\text{-}247}$-FM, its

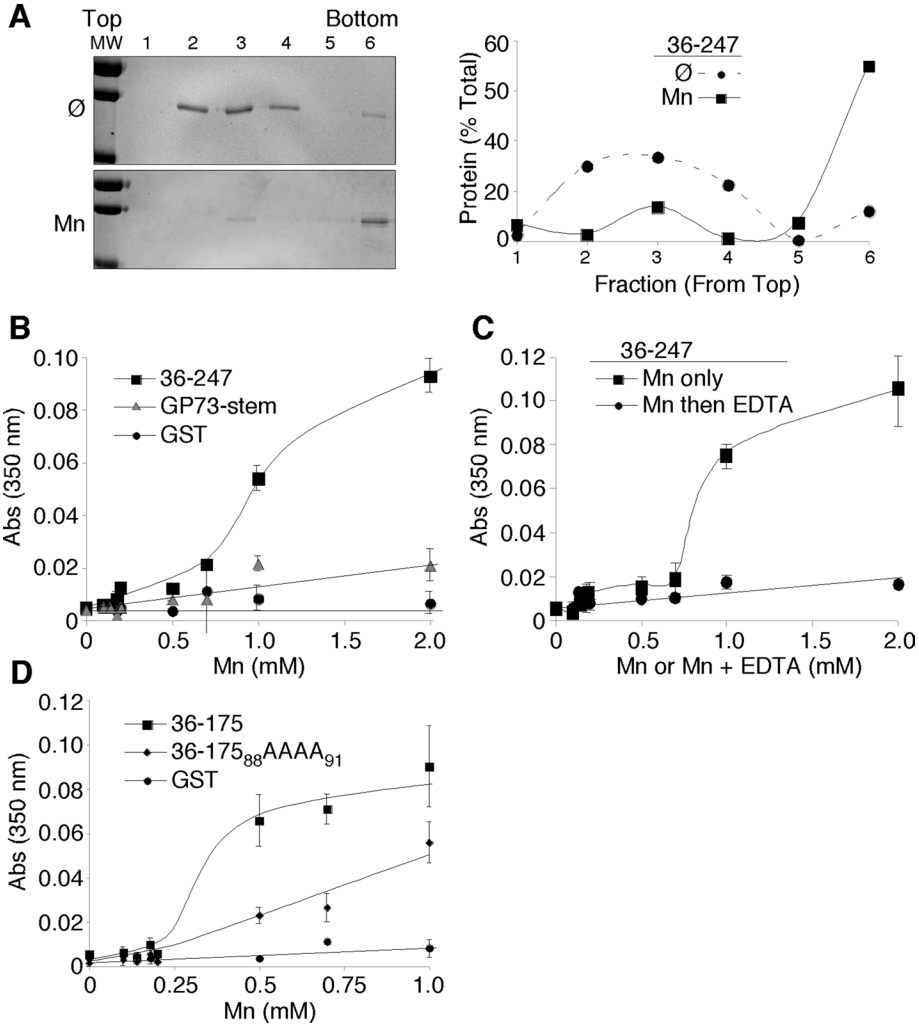

FIGURE 3: Oligomerization of the purified lumenal stem domain. (A) Coomassie-stained gel and quantification indicating recovery of purified GST-tagged residues 36–247 after velocity gradient centrifugation in the absence or presence of 1 mM $MnCl_2$. Result is representative of three independent trials. (B) Light scattering as indicated by absorbance at 350 nm at the indicated concentrations of $MnCl_2$ for purified GST-tagged residues 36–247 of GPP130, GST-tagged GP73 stem domain, or GST alone ($n = 5$, ±SEM). (C) Light scattering after incubation at the indicated concentrations of $MnCl_2$ for 10 min, followed by incubation for another 10 min with either no addition or addition of equimolar EDTA to chelate and reverse the effect of Mn binding ($n = 3$, ±SEM). (D) Light scattering for purified GST-tagged 36–175, 36–175 with the $_{88}AAAA_{91}$ substitution, and GST alone ($n = 3$, ±SEM).

expression in the presence of AP yielded stable Golgi localization, and within 30 min of drug washout, it was evident in endosome-like peripheral punctae (Figure 6A). The redistribution continued until GPP130-$_{1\text{-}247}$-FM had disappeared altogether, indicating degradation in lysosomes. Quantification of the redistribution to peripheral structures (Figure 6B) and of the loss of fluorescence (Figure 6C) confirmed a rapid and complete response. By comparison, giantin in the same cells remained Golgi localized throughout. Thus induced oligomerization of GPP130 is sufficient to alter its sorting such that it traffics out of the Golgi and is degraded.

DISCUSSION

Mn-induced GPP130 down-regulation provides an avenue to protect cells against fatal invasion by Shiga toxin. Here we asked whether GPP130 down-regulation involves Mn binding to GPP130. This seemed possible because GPP130 down-regulation requires elevated Mn inside the Golgi and involves a lumenal GPP130 sequence element that is transferable. Indeed, a purified version of this sequence element bound Mn, and mutations that blocked binding also blocked GPP130 down-regulation. Significantly, the mechanism of Mn-regulated sorting appeared to involve Mn-induced GPP130 oligomerization because Mn caused oligomerization of the purified GPP130 sequence element, Mn treatment of cells increased sedimentation of GPP130 on velocity gradients, and Mn reduced GPP130 diffusion in Golgi membranes of living cells. Each of these Mn-induced changes was blocked by alanine substitutions that interfered with Mn binding to GPP130. Further, appending an AP-regulated oligomerization motif to GPP130 yielded an independent demonstration of oligomerization-induced GPP130 down-regulation. Maturation, which is a prevailing model for membrane flux in the Golgi (Emr *et al.*, 2009), stipulates that localization of Golgi residents depends on their capture by small retrieval vesicles. Oligomerization could interfere with this process, causing progression of the oligomerized complex together with the membranes of the maturing cisternae. This would move GPP130 to the TGN, where, under these conditions, it would then be directed toward lysosomes, perhaps by default. Thus, in this view, Mn controls GPP130 down-regulation by regulating its access to cisternal maturation.

A detailed description of Mn binding by the GPP130 stem domain is an important future direction. Although atypical, metallo-coiled-coil complexes can be formed (Chakraborty *et al.*, 2010; Berwick *et al.*, 2014). It will be significant to see whether Mn binding by GPP130 shares any features with these or other metal-binding proteins. The stoichiometry of Mn binding to GPP130 is unknown. In addition, although the aspartic acid in the DFLV sequence could be an Mn coordination site, mutating only this residue did not block the GPP130 response. Binding of Mn by GPP130 is relatively weak, taking place at >100 µM. Therefore our experiments suggest that SPCA1 pumping activity brings Golgi Mn to this level during the GPP130 response, which can be initiated by extracellular Mn concentrations as low as 50 µM or less (Mukhopadhyay *et al.*, 2010; Masuda *et al.*, 2013). Golgi enzymes that use Mn as a cofactor bind Mn with relatively high affinity and are presumably metal bound under normal conditions. In contrast, under these conditions, GPP130 remains Golgi localized, implying it has a lower-affinity Mn interaction. Whereas high-affinity sites typically involve extensive coordination of their bound metal ions, an interesting implication of a low-affinity interaction is that it may be achieved by an individual GPP130 dimer that only partially coordinates its bound Mn ion. This possibility is consistent with the observation that GPP130 readily binds Mn that is already bound to NTA (Figure 2), and it also

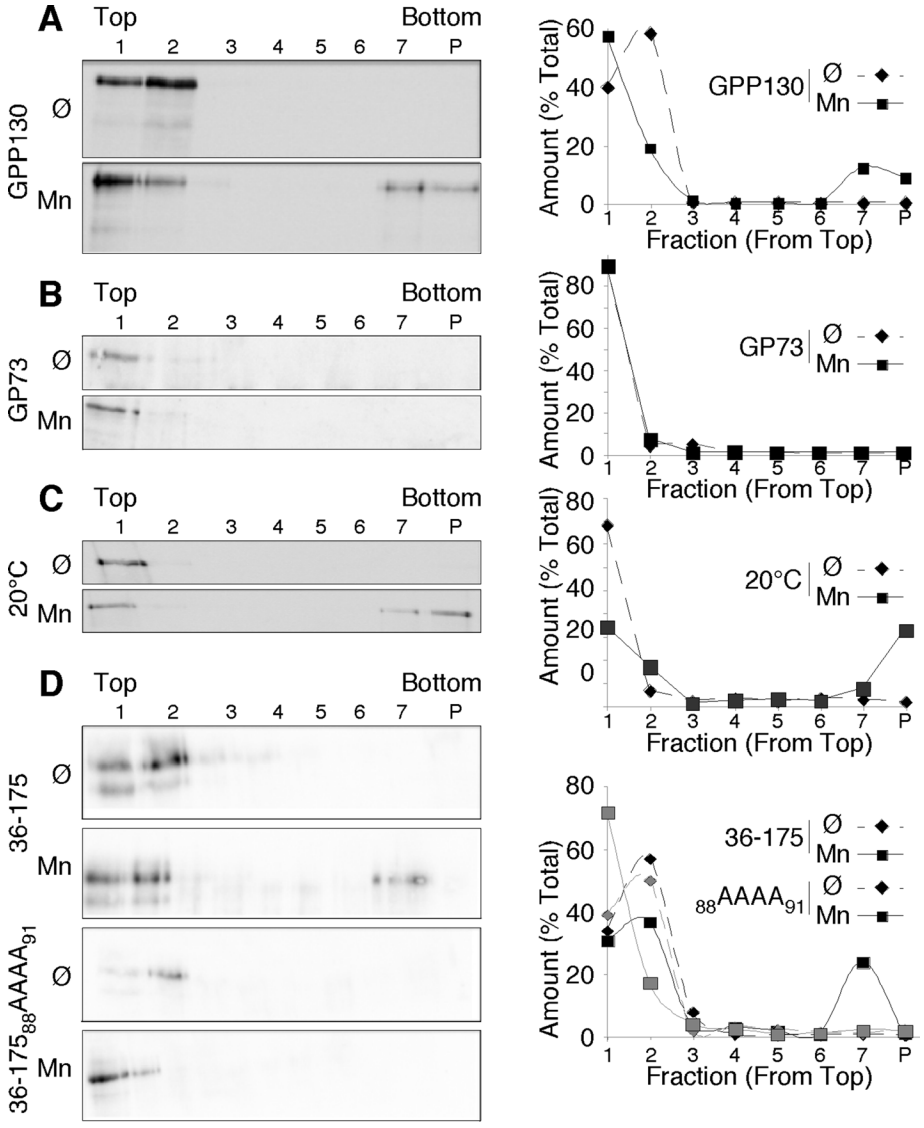

FIGURE 4: Mn-induced oligomerization of Golgi GPP130. (A) Immunoblots using anti-GPP130 antibodies to detect endogenous GPP130 after velocity gradient fractionation of detergent-solubilized cell lysates. Cells were either untreated (Ø) or treated with 0.5 mM $MnCl_2$ for 3 h (Mn), followed by cross-linking with 0.5 mM DSP. The quantified distribution profile is also shown. The entirety of each fraction was analyzed, including the resuspended pellet (P). Gradients did not contain Mn. Results are representative of three trials. (B) Immunoblot and quantified profile using anti-GP73 to detect endogenous GP73 in an identical experiment. Results are representative of three trials. (C) Immunoblot to detect endogenous GPP130 in an identical experiment, except that the 3-h incubation (with or without Mn) was carried out at 20°C to arrest GPP130 in the TGN. Results are representative of three trials. (D) Immunoblot detection of transfected GP73 chimeric constructs containing GPP130 residues 36–175 without or with the $_{88}AAAA_{91}$ substitution. Exactly as before, the cells were untreated or Mn treated, subjected to crosslinking, lysed, and fractionated on velocity gradients. The quantified fractionation profiles are also shown. Results are representative of three trials.

suggests a possible mechanism of Mn-induced oligomerization. That is, inside the Golgi, single Mn ions may simultaneously bind and link distinct GPP130 coiled-coils, thereby becoming fully coordinated and in the process clustering GPP130 dimers into large complexes in the membrane.

Many studies hinted at a functional link between aggregation and sorting. Aggregation could concentrate proteins into microdomains and also increase the ratio of sorted protein to sorting receptor. One example is regulated secretion in endocrine cells, where peptide hormones form paracrystalline arrays that are packaged into dense-core granules (Freedman and Scheele, 1993; Shennan *et al.*, 1994; Colomer *et al.*, 1996). Granule formation is initiated in the TGN, the likely location of sorting of Mn-induced GPP130 oligomers toward lysosomes, raising the question of how GPP130 behaves in response to Mn in endocrine cells. It is important to note that although purified GPP130 can homo-oligomerize (Figure 3), the GPP130 complexes that form in cells may or may not include other proteins. Another example is oligomerization-dependent apical sorting. The neurotrophin receptor p75 requires transmembrane residues for dimerization and higher-order oligomer formation, and mutation of these sites prevents its apical sorting (Youker *et al.*, 2013). Perhaps the most relevant example of aggregation-induced sorting is that reported for the protein convertase furin, which resides in the TGN. Furin is activated by its own processing in the TGN (Anderson *et al.*, 1997). The resulting product is somewhat prone to aggregation, and conditions that accelerate its aggregation cause its degradation in lysosomes (Wolins *et al.*, 1997). Intriguingly, it is believed that the furin stem domain is critical to this sorting behavior. Whether this and the Mn-induced change in GPP130 sorting are part of a quality control pathway in which aggregated proteins in the Golgi are targeted for degradation remains a significant question.

How might GPP130 oligomers be directed toward lysosomes, whereas the normal dimeric protein undergoes endosome cycling and retrieval? As mentioned, the first step might involve steric constraints that prevent large protein complexes from accessing small vesicles. If most paths out of the TGN involve sterically restricted sorting, Mn-bound GPP130 would have few options for exit from the TGN. Perhaps there is a type of default for such complexes in which the membranes acquire targeting machinery for traffic toward lysosomes. Alternatively, GPP130 oligomer formation may unmask or generate a targeting signal that promotes its active sorting into a lysosome-directed pathway. It will be important to determine the sorting factors involved on both sides of the membrane. It is known that rab7 is required and that if ubiquitination is involved, it must occur on some other protein because the GPP130 cytoplasmic domain is not required (Mukhopadhyay *et al.*, 2010). A final possibility is that GPP130 oligomerization directly alters partitioning of the protein in the TGN, perhaps via lipid interactions, so that it gains access to the lysosome pathway. However, the observation that Mn-induced GPP130 degradation maps to the stem domain rather than the transmembrane domain argues against this possibility.

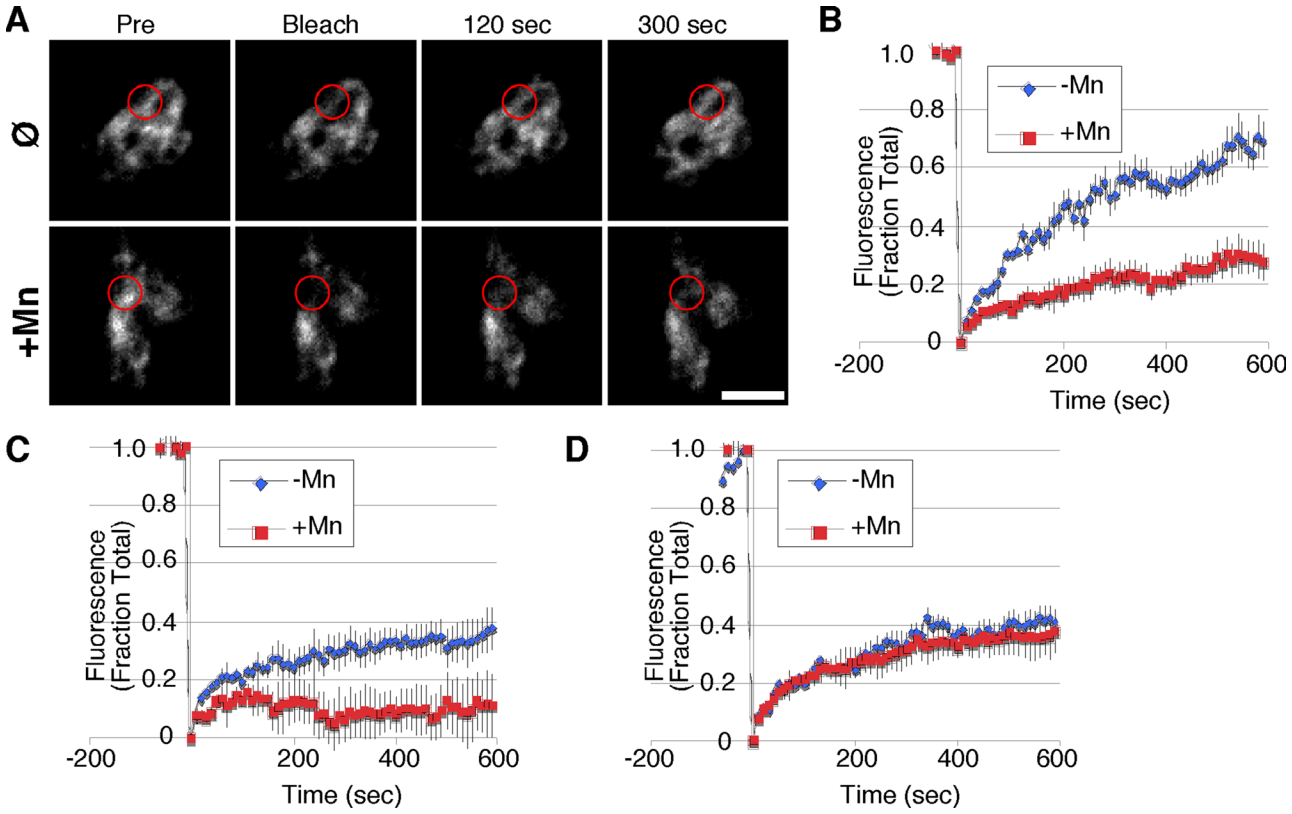

FIGURE 5: Mn slows diffusion of GPP130 in the Golgi. (A) Fluorescence images of GPP130 tagged with GFP in untreated or Mn-treated cells immediately before a small zone of the Golgi was bleached and 0, 2, and 5 min after the bleaching. Circles indicate the position and average apparent size of the bleaching. Bar, 5 μm. (B) Quantified fluorescence levels of GPP130-GFP in the bleached zone at time points before and after bleaching for untreated and Mn-treated cells ($n \geq 10$, ±SEM). (C) Quantified fluorescence levels of the chimeric GP73-GPP130 construct containing the wild-type GPP130 segment 36–175 in the bleached zone at time points before and after bleaching for untreated and Mn-treated cells ($n \geq 10$, ±SEM). (D) Quantified fluorescence levels of the chimeric GP73-GPP130 construct containing the $_{88}$AAAA$_{91}$ substitution in the GPP130 segment 36–175 in the bleached zone at time points before and after bleaching for untreated and Mn-treated cells ($n \geq 10$, ±SEM).

The function of GPP130 remains unknown, but few, if any, other proteins are down-regulated by Mn, and Mn is the only divalent ion that causes this effect (Mukhopadhyay *et al.*, 2010). On this basis, our working hypothesis is that GPP130 is involved in Mn homeostasis. For example, it could be a negative regulator of components involved in reducing cytoplasmic Mn. One mechanism of Mn control involves its sequestration in the Golgi, followed by secretion (Culotta *et al.*, 2005; Mukhopadhyay and Linstedt, 2011). When extracellular Mn is low, activities such as SPCA1-mediated movement of Mn into the Golgi may be dampened to maintain basal levels of Mn in the cytoplasm. On increased Mn load, these activities might be up-regulated to protect against toxic cytoplasmic concentrations. Thus when Mn reaches a high level in the Golgi it binds GPP130, causing GPP130 down-regulation, which, in turn, would accelerate Mn sequestration and secretion. So far, GPP130 has not been shown to interact with SPCA1 or other Golgi components.

In closing, the purpose of Mn-induced GPP130 degradation remains a future issue, but because GPP130 is used by Shiga toxin to invade cells, Mn-induced GPP130 degradation presents itself as a possible inexpensive and readily available therapy for a devastating disease. Mn-induced GPP130 degradation also provides a paradigm for regulation of membrane trafficking. Our results indicate that GPP130 contains a coiled-coil Mn-binding domain that senses elevated concentrations of Mn in the Golgi lumen. On Mn binding, GPP130 undergoes oligomerization that is necessary and sufficient to direct the protein to lysosomes, where it is degraded. Future work may reveal that the GPP130 response evolved for the purpose of Mn homeostasis and that the mechanism of down-regulation makes use of a preexisting quality control pathway.

MATERIALS AND METHODS

Antibodies and other reagents

Polyclonal antibodies against GPP130 and giantin (Mukhopadhyay *et al.*, 2010) and monoclonal antibodies against GPP130 and GFP were described (Puri *et al.*, 2002; Mukhopadhyay *et al.*, 2010). Horseradish peroxidase–conjugated goat anti-rabbit or anti-mouse secondary antibodies were used at 1:3000 for immunoblots (Bio-Rad, Hercules, CA). Alexa Fluor 488 and Alexa Fluor 568 (Invitrogen, Carlsbad, CA) were used as secondary antibodies at 1:400 for immunofluorescence. DSP was from Thermo Scientific (Waltham, MA). AP (now called D/D solubilizer) was purchased from Clontech (Mountain View, CA). Unless noted, other chemicals were from Fisher (Fisher Scientific, Hanover Park, IL).

Cell culture and transfections

HeLa cells were grown in MEM with 100 IU/ml penicillin G and 100 μg/ml streptomycin supplemented with 10% fetal bovine serum (Atlanta Biologicals, Lawrenceville, GA) and maintained at 37°C in a 5% CO_2 incubator. For 20°C incubations, the cells were floated on a 20°C water bath in a cold room. For Mn treatment, culture medium

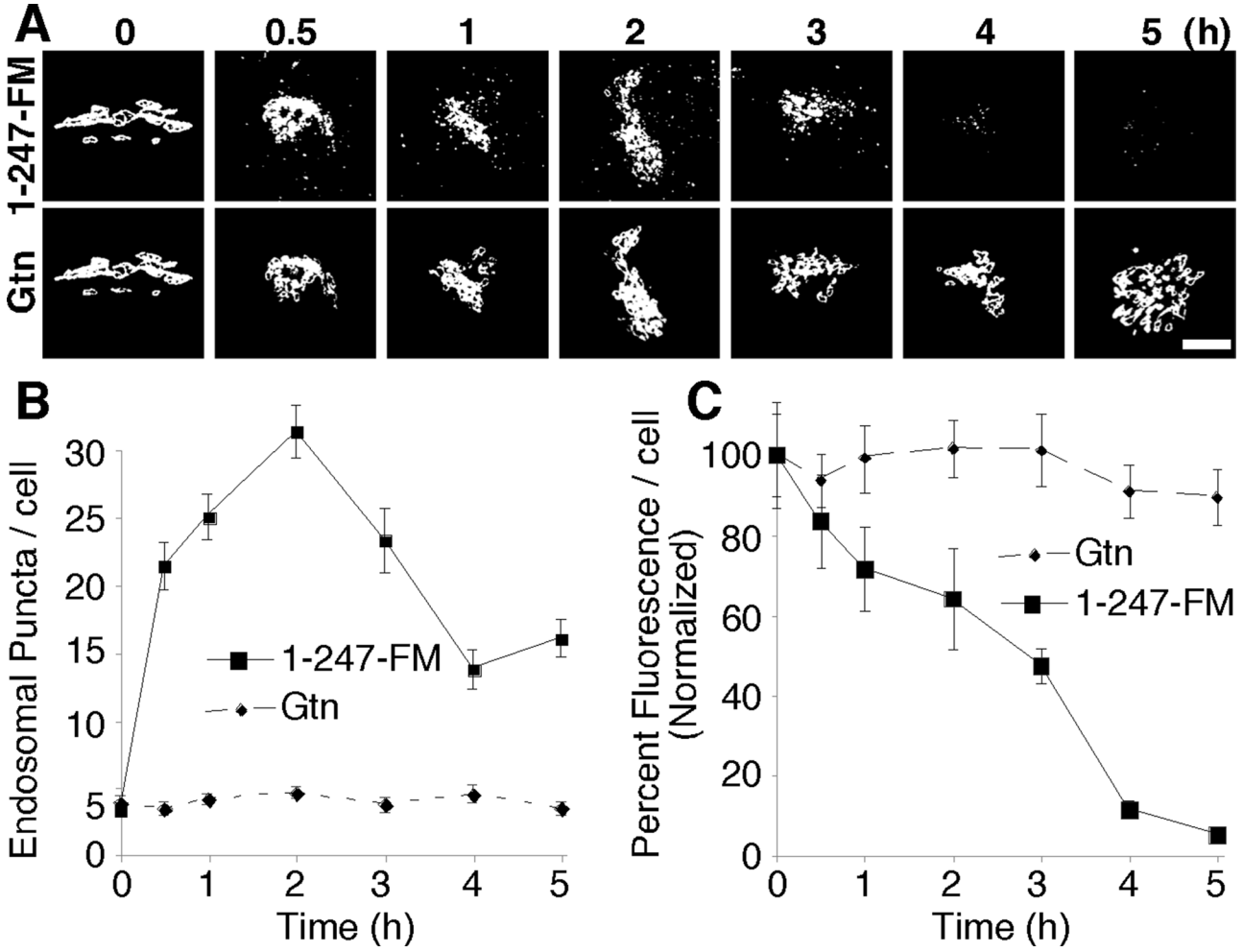

FIGURE 6: Forced GPP130 oligomerization causes loss of Golgi localization and degradation. (A) Thresholded fluorescence images of GPP130 tagged with the FM oligomerization domain (1-247-FM) in cells at the indicated times after AP washout to induce oligomerization. The Golgi marker giantin (Gtn) is shown in the same cells. Bar, 2 μm. (B) Quantified number of fluorescent puncta per cell for 1-247-FM and giantin at various times of AP washout ($n = 3$, ±SEM). (C) Quantified total fluorescence signal per cell for 1-247-FM and giantin at various times of AP washout ($n = 3$, ±SEM).

was adjusted to the desired concentration using a freshly prepared 1 M stock of $MnCl_2$ in sterile water. DNA transfections were performed using the JetPEI transfection reagent (PolyPlus, Illkirch, France) according to the manufacturer's protocol. Cultures were transfected 24 h after plating and, unless noted otherwise, used for experiments 24 h after transfection.

Constructs

Chimeric constructs GP73-GPP130$_{36\text{-}175}$-GFP and GP73-GPP130$_{36\text{-}87}$-GFP were described (Mukhopadhyay *et al.*, 2010). GP73-GPP130$_{36\text{-}107}$-GFP, GP73-GPP130$_{36\text{-}100}$-GFP, GP73-GPP130$_{36\text{-}95}$-GFP, GP73-GPP130$_{50\text{-}100}$-GFP, and GP73-GPP130$_{60\text{-}100}$-GFP were created from the parent construct GP73-GPP130$_{36\text{-}175}$-GFP using a PCR-based loop-out modification of the QuikChange protocol (Stratagene, La Jolla, CA). Briefly, a 5′ forward primer was designed to anneal with 18–21 base pairs on both sides flanking the region to be deleted, thus creating the loop-out. A 3′ reverse primer (18–21 base pairs) was designed to anneal with a strand complementary to 3′ end of the forward primer. Forward and reverse primers were designed to contain either a guanine or cytosine at each end to increase annealing. Alanine substitutions in GP73-GPP130$_{36\text{-}95}$-GFP and GP73-GPP130$_{36\text{-}175}$-GFP were introduced using the loop-out modification. All constructs maintained the integrity of the predicted coiled-coil structure based on analysis using the COILS program (www.ch.embnet.org/software/COILS_form.html). Previous work described the generation of GST-GPP130$_{36\text{-}247}$, GST-GPP130$_{36\text{-}175}$, GST-GPP130$_{36\text{-}87}$ (Mukhopadhyay *et al.*, 2012), and GST-GP73$_{36\text{-}195}$ (Bachert *et al.*, 2007). GST-GPP130$_{36\text{-}175}$ (containing the $_{88}$AAAA$_{91}$ substitution) was generated using the loop-out modification. GPP130$_{1\text{-}247}$-FM-GFP was generated by subcloning the FM domain (from Man1-FM-HA; Rizzo *et al.*, 2013) in frame after the codon for residue 247 of GPP130 and before the GFP sequence using restriction sites. All constructs were confirmed by restriction analysis and sequencing.

Trafficking assay

Approximately 24 h posttransfection, the medium was adjusted to 100 μg/ml cycloheximide for 2 h and then adjusted to 500 μM $MnCl_2$ for another 2 h. The cells were then fixed and analyzed by immunofluorescence to detect GFP and endogenous GPP130 as described later.

Protein purification and Mn binding assays

GST and GST fusion proteins were expressed and purified from bacteria as described (Guo *et al.*, 2008). The purified proteins were dialyzed into phosphate-buffered saline (PBS) at pH 7.4 containing

0.1% β-mercaptoethanol or Good's buffer (10 mM 4-(2-hydroxyethyl)-1-piperazineethanesulfonic acid, 115 mM NaCl, 2.4 mM K_2HPO_4, pH 7.4) with 0.1% β-mercaptoethanol. Stripped NTA-agarose beads were generated by washing Ni-NTA agarose beads (Invitrogen) with five volumes of water and three volumes of 2% SDS, followed by a dehydration/rehydration series of one volume each of 25, 50, and 75% EtOH, five volumes of 100% EtOH, one volume of 75, 50, and 25% EtOH, five volumes of water, and then five volumes of 100 mM EDTA, pH 8.0 (http://kirschner.med.harvard.edu/files/protocols/QIAGEN_QIAexpressionist_EN.pdf). Color change (blue to white) accompanied removal of Ni. The stripped NTA-agarose beads were then rotated with 50 mM $MnCl_2$ for 1 h at 4°C, followed by centrifugation and resuspension in water in preparation for use the same day. For binding, either 10 µl of Mn beads were washed and incubated with 10 µg of the indicated protein in PBS or 5 µl of Mn beads were washed and incubated with 0.5 µg of the indicated protein in Good's buffer. The reaction (50-µl total volume) was rotated for 30 min at 4°C. Beads were collected and twice washed with binding buffer containing 0.1% Triton X-100 using pulse spins and aspiration of the supernatants with a 25-gauge needle. A final wash with binding buffer only was followed by boiling in reducing sample buffer, SDS–PAGE, Coomassie staining, image capture (Fujifilm Luminescent Image Analyzer, LAS-3000; Fujifilm, Tokyo, Japan) and quantification using ImageJ (National Institutes of Health, Bethesda, MD). To determine the concentration dependence of binding, 5-µl aliquots of stripped NTA-agarose beads were rotated with various concentrations of $MnCl_2$ for 1 h at 4°C and then supplemented with 0.5 µg of GST-GPP130$_{36\text{-}247}$ and rotated for an additional 30 min at 4°C. Binding was carried out in Good's buffer with a 30-µl reaction volume, achieving the indicated final $MnCl_2$ concentration. Washing and analysis were as before, except that nonlinear regression analysis was performed using Prism (GraphPad Software, La Jolla, CA).

Light scattering assay

Purified proteins (5 µM, 10 µl final volume) were incubated with various concentrations of $MnCl_2$ for 5 min at room temperature in either PBS or Good's buffer. Absorbance was then determined at 360 nm using ND-1000 UV-Vis spectrophotometer (NanoDrop, Wilmington, DE). For the reversibility test, after the initial 5 min, an equal concentration of EDTA was added for an additional 5 min.

Velocity gradient sedimentation assays

Purified proteins (10 µg) were layered on top of sucrose gradients prepared in PBS with or without 1 mM $MnCl_2$ and consisting of a 1-ml 40% cushion overlaid with 1-ml steps of 22.5 and 10%. Centrifugation was at 55,000 rpm in a SW50.1 rotor (Beckman Coulter) for 12 h at 4°C. Fractions (500 µl) were collected from the top with a pipette and analyzed by Coomassie and quantified as described (Mukhopadhyay *et al.*, 2013). For cell extract analysis, transfected or control cells were treated with 0 or 500 µM Mn for 3 h at 37°C. For each gradient, cells in two 10-cm dishes were then washed with PBS, trypsinized, collected by centrifugation for 2 min at 450 × *g*, and resuspended in 500 µl PBS, which was then adjusted to 0.5 mM DSP and rotated at 37°C for 45 min. The reaction was quenched by adjustment to 50 mM Tris on ice for 15 min. For cells exposed to Mn at 20°C, the extracts were prepared in the same way, except that they were removed from plates by scraping while on ice, and the cross-linking was carried out at 20°C. After quenching, the cells were collected and lysed in RIPA buffer (25 mM, pH 7.4; 150 mM NaCl, 1% NP-40, 0.5% sodium deoxycholate, 0.1% SDS and 0.1% β-mercaptoethanol, 10 µg/ml leupeptin, 10 µg/ml pepstatin, and 1 mM phenylmethylsulfonyl fluoride), using 50 passes through a 25-gauge needle. The extract was clarified in a microfuge at 15,000 rpm for 15 min at 4°C and layered on a 10–40% linear sucrose gradient in RIPA buffer. Centrifugation was at 50,000 rpm in the SW50.1 rotor for 1.5 h at 4°C. Fractions (500 µl) were collected from the bottom using tubing and a peristaltic pump. Remaining material at the bottom was resuspended in RIPA buffer. Immunoblot analysis was carried out on 20% of each fraction and the entire pellet using enhanced chemiluminescence, image capture (Fujifilm Luminescent Image Analyzer, LAS-3000), and quantification (ImageGauge software, Fujifilm).

Controlled polymerization

Cells were transfected with GPP130$_{1\text{-}247}$-FM-GFP, and after 16–18 h they were placed in fresh medium containing 1 µM AP for 24 h, followed by another change to medium containing 1 µM AP and 100 µg/ml cycloheximide for 30 min. Next the cells were incubated in medium containing only 100 µg/ml cycloheximide for various times before fixation and imaging. Only cells exhibiting moderate expression levels were analyzed.

Microscopy

Immunofluorescence was performed on cells fixed with 3% paraformaldehyde as described (Mukhopdhyay *et al.*, 2010) using Alexa Fluor 488 and 568 secondary antibodies (Invitrogen). Images were captured using a spinning-disk confocal scan head microscope equipped with a three-line laser (Excelitas Technologies, Waltham, MA), independent excitation and emission filter wheels (PerkinElmer Life and Analytical Sciences, Boston, MA), and a 12-bit Orca ER digital camera (Hamamatsu Photonics, Bridgewater, NJ) mounted on an Axiovert 200 microscope with a 100×, 1.4 numerical aperture oil immersion objective (Carl Zeiss, Thornwood, NY). Sections encompassing the cells were acquired at 0.3-µm steps using MicroManager software (www.micromanager.org/). To highlight cytoplasmic puncta, images presented in the figures are maximum value projections that have been uniformly thresholded after background subtraction. FRAP experiments were carried out with the Andor iQ2 spinning-disk confocal system (Andor, Belfast, United Kingdom). Stacks of *Z*-slices were acquired at 10-s intervals for 1 min before photobleaching to establish a baseline. GFP was bleached using 27.3 mW of 488-nm laser power for 20 µs/pixel repeated 60 times. Fluorescence recovery was followed at 10-s intervals for 10 min after photobleaching.

Image analysis

Immunofluorescence images were analyzed using ImageJ as described (Mukhopadhyay *et al.*, 2010). To measure fluorescence per cell, background was subtracted from each *Z*-section, and average value projections were created. Cells were outlined using the Gaussian blur filter, and mean fluorescence was measured using the Measure plug-in of ImageJ. The number of cytoplasmic punctae per cell was determined using the Analyze Particle plug-in of ImageJ (particle range setting of 10–100 pixels) from maximum value projections that were uniformly thresholded after background subtraction. FRAP analysis in ImageJ was performed on average *Z*-projections of background-subtracted slices. The total fluorescence value within the bleached region of interest (Roi) was normalized to the total cellular fluorescence (Total) at each time point to correct for photobleaching due to imaging using the following equation:

$$\text{FRAP normalization} = \left(\frac{\text{Roi}_{(n)}/\text{Roi}_{(-1)}}{\text{Total}_{(n)}/\text{Total}_{(-1)}} - \frac{\text{Roi}_{(0)}/\text{Roi}_{(-1)}}{\text{Total}_{(0)}/\text{Total}_{(-1)}}\right) \div \left(1 - \frac{\text{Roi}_{(0)}/\text{Roi}_{(-1)}}{\text{Total}_{(0)}/\text{Total}_{(-1)}}\right)$$

ACKNOWLEDGMENTS

We thank members of the Linstedt lab for their help, especially Collin Bachert and Somshuvra Mukhopadhyay (now at the University of Texas, Austin, Texas) for help with construct generation and assay development, respectively. For critical advice, we thank Tina H. Lee, Manojkumar A. Puthenveedu, and Michael P. Hendrich (Carnegie Mellon, Pittsburgh, PA), as well as Patrick Thibodeau (University of Pittsburgh, Pittsburgh, PA). Man1-FM-HA was a generous gift from Alberto Luini (Consiglio Nazionale delle Ricerche, Naples, Italy). This project was funded by National Institutes of Health R01 Grant GM08411101 (to A.D.L.).

REFERENCES

Anderson ED, VanSlyke JK, Thulin CD, Jean F, Thomas G (1997). Activation of the furin endoprotease is a multiple-step process: requirements for acidification and internal propeptide cleavage. EMBO J 16, 1508–1518.

Bachert C, Fimmel C, Linstedt AD (2007). Endosomal trafficking and proprotein convertase cleavage of cis Golgi protein GP73 produces marker for hepatocellular carcinoma. Traffic 8, 1415–1423.

Beddoe T, Paton AW, Le Nours J, Rossjohn J, Paton JC (2010). Structure, biological functions and applications of the AB5 toxins. Trends Biochem Sci 35, 411–418.

Berwick MR, Lewis DJ, Jones AW, Parslow RA, Dafforn TR, Cooper HJ, Wilkie J, Pikramenou Z, Britton MM, Peacock AF (2014). De novo design of Ln(III) coiled coils for imaging applications. J Am Chem Soc 136, 1166–1169.

Borgstahl GE, Parge HE, Hickey MJ, Beyer WF Jr, Hallewell RA, Tainer JA (1992). The structure of human mitochondrial manganese superoxide dismutase reveals a novel tetrameric interface of two 4-helix bundles. Cell 71, 107–118.

Chakraborty S, Touw DS, Peacock AF, Stuckey J, Pecoraro VL (2010). Structural comparisons of apo- and metalated three-stranded coiled coils clarify metal binding determinants in thiolate containing designed peptides. J Am Chem Soc 132, 13240–13250.

Colomer V, Kicska GA, Rindler MJ (1996). Secretory granule content proteins and the luminal domains of granule membrane proteins aggregate in vitro at mildly acidic pH. J Biol Chem 271, 48–55.

Cromwell ME, Hilario E, Jacobson F (2006). Protein aggregation and bioprocessing. AAPS J 8, E572–E579.

Culotta VC, Yang M, Hall MD (2005). Manganese transport and trafficking: lessons learned from *Saccharomyces cerevisiae*. Eukaryot Cell 4, 1159–1165.

Emr S, Glick BS, Linstedt AD, Lippincott-Schwartz J, Luini A, Malhotra V, Marsh BJ, Nakano A, Pfeffer SR, Rabouille C, *et al*. (2009). Journeys through the Golgi—taking stock in a new era. J Cell Biol 187, 449–453.

Endo Y, Tsurugi K, Yutsudo T, Takeda Y, Ogasawara T, Igarashi K (1988). Site of action of a Vero toxin (VT2) from *Escherichia coli* O157:H7 and of Shiga toxin on eukaryotic ribosomes. RNA N-glycosidase activity of the toxins. Eur J Biochem 171, 45–50.

Fraser ME, Chernaia MM, Kozlov YV, James MN (1994). Crystal structure of the holotoxin from *Shigella dysenteriae* at 2.5 A resolution. Nat Struct Biol 1, 59–64.

Freedman SD, Scheele GA (1993). Regulated secretory proteins in the exocrine pancreas aggregate under conditions that mimic the *trans*-Golgi network. Biochem Biophys Res Commun 197, 992–999.

Guo Y, Punj V, Sengupta D, Linstedt AD (2008). Coat-tether interaction in Golgi organization. Mol Biol Cell 19, 2830–2843.

Jensen LT, Carroll MC, Hall MD, Harvey CJ, Beese SE, Culotta VC (2009). Down-regulation of a manganese transporter in the face of metal toxicity. Mol Biol Cell 20, 2810–2819.

Johannes L, Wunder C (2011). Retrograde transport: two (or more) roads diverged in an endosomal tree? Traffic 12, 956–962.

La Fontaine S, Mercer JF (2007). Trafficking of the copper-ATPases, ATP7A and ATP7B: role in copper homeostasis. Arch Biochem Biophys 463, 149–167.

Mallard F, Johannes L (2003). Shiga toxin B-subunit as a tool to study retrograde transport. Methods Mol Med 73, 209–220.

Masuda M, Braun-Sommargren M, Crooks D, Smith DR (2013). Golgi phosphoprotein 4 (GPP130) is a sensitive and selective cellular target of manganese exposure. Synapse 67, 205–215.

Mukhopadhyay S, Bachert C, Smith DR, Linstedt AD (2010). Manganese-induced trafficking and turnover of the *cis*-Golgi glycoprotein GPP130. Mol Biol Cell 21, 1282–1292.

Mukhopadhyay S, Linstedt AD (2011). Identification of a gain-of-function mutation in a Golgi P-type ATPase that enhances Mn2 +efflux and protects against toxicity. Proc Natl Acad Sci USA 108, 858–863.

Mukhopadhyay S, Linstedt AD (2012). Manganese blocks intracellular trafficking of Shiga toxin and protects against Shiga toxicosis. Science 335, 332–335.

Mukhopadhyay S, Linstedt AD (2013). Retrograde trafficking of AB(5) toxins: mechanisms to therapeutics. J Mol Med (Berl) 91, 1131–1141.

Mukhopadhyay S, Redler B, Linstedt AD (2013). Shiga toxin-binding site for host cell receptor GPP130 reveals unexpected divergence in toxin-trafficking mechanisms. Mol Biol Cell 24, 2311–2318.

Polishchuk R, Lutsenko S (2013). Golgi in copper homeostasis: a view from the membrane trafficking field. Histochem Cell Biol 140, 285–295.

Puri S, Bachert C, Fimmel CJ, Linstedt AD (2002). Cycling of early Golgi proteins via the cell surface and endosomes upon lumenal pH disruption. Traffic 3, 641–653.

Reddi AR, Jensen LT, Culotta VC (2009). Manganese homeostasis in *Saccharomyces cerevisiae*. Chem Rev 109, 4722–4732.

Rizzo R, Parashuraman S, Mirabelli P, Puri C, Lucocq J, Luini A (2013). The dynamics of engineered resident proteins in the mammalian Golgi complex relies on cisternal maturation. J Cell Biol 201, 1027–1036.

Sandvig K, Bergan J, Dyve AB, Skotland T, Torgersen ML (2010). Endocytosis and retrograde transport of Shiga toxin. Toxicon 56, 1181–1185.

Shennan KI, Taylor NA, Docherty K (1994). Calcium- and pH-dependent aggregation and membrane association of the precursor of the prohormone convertase PC2. J Biol Chem 269, 18646–18650.

Sullivan JA, Lewis MJ, Nikko E, Pelham HR (2007). Multiple interactions drive adaptor-mediated recruitment of the ubiquitin ligase rsp5 to membrane proteins in vivo and in vitro. Mol Biol Cell 18, 2429–2440.

Wolins N, Bosshart H, Kuster H, Bonifacino JS (1997). Aggregation as a determinant of protein fate in post-Golgi compartments: role of the luminal domain of furin in lysosomal targeting. J Cell Biol 139, 1735–1745.

Youker RT, Bruns JR, Costa SA, Rbaibi Y, Lanni F, Kashlan OB, Teng H, Weisz OA (2013). Multiple motifs regulate apical sorting of p75 via a mechanism that involves dimerization and higher-order oligomerization. Mol Biol Cell 24, 1996–2007.